In vitro pulmonary toxicity of thermally processed titania nanotubes

Saoirse Dervin[1, 5] Eugen Panaitescu[3], Latika Menon[3], Steven S. Hinder[4], Suresh C. Pillai[1, 5] and Mary Garvey[* 1, 2],

[1]Centre for Precision Engineering, Materials and Manufacturing Research (PEM), Institute of Technology, Sligo, Ireland

[2]Cellular Health and Toxicology Research Group, Institute of Technology Sligo, Sligo, Ireland

[3]Department of Physics, Northeastern University, Boston, MA 02115, United States

[4]The Surface Analysis Laboratory, Faculty of Engineering and Physical Sciences, University of Surrey, Guildford, Surrey, GU2 7XH, United Kingdom

[5]Nanotechnology and Bio-Engineering Research Group, Department of Environmental Science, Institute of Technology Sligo, Ireland

*Corresponding author:

Email: garvey.mary@itsligo.ie

Department of Life Sciences

Institute of Technology Sligo

Ash Lane, Sligo

Ireland

Phone: +353719305841

Cite this article as Dervin, Saoirse, Eugen Panaitescu, Latika Menon, Steven S. Hinder, Suresh C. Pillai, and Mary Garvey. "In vitro pulmonary toxicity of thermally processed titania nanotubes." *Journal of Nanoparticle Research* 22, no. 1 (2020): 1-15. https://doi.org/10.1007/s11051-019-4722-z

Abstract

The current study examined the *in vitro* pulmonary toxicity of titania nanotubes (TNTs) induced by the morphological and crystalline changes associated with post-synthetic thermal processing. A549 lung carcinoma cells were exposed to untreated, amorphous TNTs and those treated at 200, 400, 600 and 800^{o}C, respectively. The cytotoxic action of the untreated and annealed TNTs was assessed using a battery of cytotoxicity assays that examined cellular metabolic and prolific activity and membrane integrity, in addition to the production of intracellular reactive oxygen species (ROS). Toxicity effects due to the period and dose of exposure were determined by exposing the A549 cell line to various TNT concentrations during different incubation periods. The untreated, amorphous and annealed TNTs elicited an overall dose dependent increase in toxicity. As the annealing temperature increased from 200-800^{o}C the nanotubular structure of TNTs fragmented and a crystalline phase composition developed. Crystalline nanoparticles also began to grow among the walls of disintegrated TNTs, and crystallite and particle size increased progressively. In comparison to amorphous TNTs, those of anatase, rutile, or anatase/rutile mixed phase composition exerted notable *in vitro* pulmonary toxicity. Rutile rich TNTs possessing fragmented nanotube walls and larger particle size induced the greatest loss in viability of A549 lung carcinoma cells, presumably due to the domination of the rigid rutile crystal arrangement. The current study thus highlights the necessity for material manufacturers to consider the effects of post-synthetic processing on the possible toxicity profile of nanomaterial containing products and devices.

Keywords: Titania nanotubes, post-synthetic thermal processing, annealing, crystallinity, anatase rutile, cell toxicity

TOC:

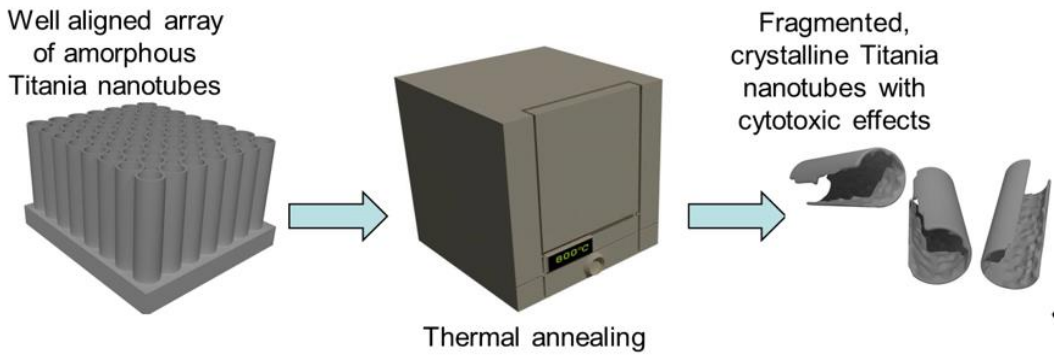

1.0 Introduction

The rapid development of nanotechnology and the unique physical and chemical properties of engineered nanomaterials have motivated their widespread use within catalytic technologies, water treatment, electronics, sensors, biomedicine, antimicrobial agents, textiles, plastic fillers and even car tires. (Chimene et al. 2015; Dervin et al. 2016; Ganguly et al. 2018; Garvey et al. 2016; Hoet et al. 2004; Hou et al. 2018; Khan et al. 2017; Masciangioli and Zhang 2003)

Nanoscale titanium dioxide (TiO_2) is one of the most widely manufactured nanomaterials. (Hendren et al. 2011) Due to their high stability, anticorrosion and photocatalytic properties, TiO_2 nanomaterials (TNMs) serve a variety of applications ranging from common products, such as sunscreens, personal care products, and cosmetics to advanced devices like photovoltaic cells. (Bai et al. 2014; Weir et al. 2012) TNMs also assist a series of environmental applications, such as photocatalytic pollutant degradation and microbial inactivation, water treatment and energy production. (Byrne et al. 2018; Nasr et al. 2018) Owing to their distinct structure-related photocatalytic properties, exceptional biocompatibility and high chemical stability, intensive experimental and theoretical investigations have also been dedicated to the biomedical implementations of TNMs, realizing applications in biosensing, drug delivery, antimicrobial coatings, etc. (Yin et al. 2013) The significance of the variety of TNM

applications has spurred substantial advances in the fabrication, characterization, and fundamental understanding of TNMs and their related technologies. (Chen and Mao 2007; Chen and Selloni 2014; Fujishima and Honda 1972; Henderson and Lyubinetsky 2013; Linsebigler et al. 1995; Zhang and Yates Jr 2012)

The exponential growth of nanotechnology has also motivated the development of innovative TiO_2 nanostructures (TNSs). A range of TNSs with different dimensionalities, such as nanoparticles, nanosheets, nanocables, nanofibers, nanowires, nanobelts, nanorods, nanotubes, and interconnected architectures, have recently been explored. (Camposeco et al. 2016; Lee et al. 2014; Wang et al. 2014; Wu et al. 2017) Although photoinduced reactions on titania nanopowders and thin films provide an effective platform for dye sensitized solar cells, hydrogen production *via* water splitting, photocatalytic self-cleaning surfaces and redox reactions, the high length/diameter aspect ratio of nanotubular titania provides high surface area and reduced interfacial boundaries, which hold special promise for many of these same applications. (Grätzel 2001; Khan et al. 2002; Mor et al. 2006; Vijayan et al. 2010; Wang et al. 1998; Zhu et al. 2007) TiO_2 nanotubes (TNTs) have also attracted considerable attention due to their low cost and ease of preparation, unique chemical and mechanical stability, ion changeable ability and reduced rate of charge recombination. (Wu et al. 2017) Due to these unique structure-related properties, the nanotubular forms of TiO_2 have found wide application in a variety of fields such as electronics, catalysis, solar energy and biomedicine. (AlHoshan et al. 2012; Kuchibhatla et al. 2007; Lee et al. 2014; Vijayan et al. 2010) Despite the promise of TNTs, the accelerated mass production, extensive use, and uncontrolled disposal of complex titania nanoforms will inevitably lead to environmental release and a potential risk to organisms and ecosystems. (Hou et al. 2019)

TNTs can be prepared using a variety of practices including template assisted methods, sol-gel processing, hydrothermal synthesis techniques and thermal or electrochemical anodic

oxidation. (Baiju et al. 2009; Ghicov et al. 2005; Hoyer 1996; Jung et al. 2002; Kasuga et al. 1998; Kasuga et al. 1999; Lee et al. 2005; Lei et al. 2001; Tsuchiya et al. 2005; Varghese et al. 2003; Vijayan et al. 2010) Anodically formed, vertically aligned TNTs were first synthesized in 1999 [6] and have since attracted great interest due to their high surface area, attractive light absorption properties and impressive chemical reactivity. In addition to their efficient electron transport, facilitated by the vertical alignment of the quasi one-dimensional (1D) structures and the effective, structure associated charge-transfer. These nanotube layers have thus proven useful for photocatalysis, catalysis, dye-sensitized solar cells, electrochromic and photochromic devices, bio-related applications, wettability control and as templates for secondary material deposition. (Albu et al. 2008; AlHoshan et al. 2012; Balaur et al. 2005; Ghicov et al. 2006; Macak et al. 2007a; Macak et al. 2007b; Paramasivam et al. 2007; Tsuchiya et al. 2006; Zhu et al. 2007)

The electronic and chemical properties, and thus performance of anodically grown TNTs are modulated by the complex interplay of various material attributes including, size, surface roughness, wall thickness, morphology, and the degree of crystallinity. (Brahmi et al. 2015; Vijayan et al. 2010; Zhu et al. 2007)

As anodized TNTs consist of amorphous structures with low conductivity and mechanical strength, all of which potentially hinder TNT performance. The properties of TNTs can be improved by grain size, microstructure, surface photoelectrochemical properties, particle morphology and phase composition. This may be achieved by various post-synthetic processes such as electrochemical, photoelectrochemical, and thermal treatments. (AlHoshan et al. 2012; Palmas et al. 2011) Post-synthetic thermal processing provides a quick, low-cost and facile route to modulate TNT physiochemical properties *via* the adjustment of experimental parameters such as temperature, time and atmospheres. (Kaneco et al. 1998; Liu et al. 2008; Yu and Wang 2010) Processes such as this are also routinely implemented in manufacturing

practices to integrate TNTs into various devices and technologies. [6] For instance, amorphous anodically grown TNTs are thermally annealed during implant manufacture to modulate structural, physical and electrochemical properties for enhanced cell proliferation and osteoconductivity. (Bhosle and Friedrich 2017; Das et al. 2009)

On the other hand, nanomaterial post-synthetic modification also poses new risks to occupational health. During post-synthetic manufacturing practices, airway surface cells, including lung cells, are the first cell type to encounter TNTs. (Magrez et al. 2009) Thermal processing also generates TNTs of various forms with different physicochemical characteristics (e.g., crystallinity, shape, particle size, surface area, and surface modification) that may possess unknown risks of pulmonary toxicity. (Fang et al. 2011; Tsai and Teng 2004; Vijayan et al. 2010; Yu and Wang 2010) Just as the toxicity of a fiber-shaped nanomaterial cannot be foretold from the known toxicity of the same material in nanoparticle form, the toxicity of processed nanomaterials cannot be predetermined from the safety profile of the unprocessed parent material.

Furthermore, TiO_2 has, until recently, been deemed biologically inert, alluding that environmental or occupational exposure was moderately undamaging. (Hamilton et al. 2009) In 2011 however, these assumptions were challenged. The US National Institute for Occupational Safety and Health (NIOSH) revised TiO_2 carcinogenetic information, concluding that "TiO_2 is not a direct-acting carcinogen, but acts through a non-specific secondary genotoxicity mechanism primarily related to particle size and surface area (CDC, 2011)." (Drobne 2018) More recently, the European Chemical Agency (ECHA) and the European Union's Registration, Evaluation, Authorisation and Restriction of Chemicals Regulation (REACH) have proposed that TiO_2 be classified as a category 2 carcinogen (suspected of causing cancer) through inhalation. (Drobne 2018; ECHA proposes classification of TiO2 as category 2 carcinogen 2017)

Despite the full measure of the above, systematic studies assessing the influences of post-synthetic processing techniques on the *in vitro* cytotoxic action of TNTs are limited. Accordingly, the current study examined the *in vitro* pulmonary toxicity of TNTs induced by the morphological and crystalline changes associated with post-synthetic thermal processing. A549 lung carcinoma cells were exposed to untreated, amorphous TNTs and those treated at 200, 400, 600 and 800^{o}C, respectively. The cytotoxic action of the untreated and annealed TNTs was assessed using a battery of cytotoxicity assays that examined cellular metabolic and prolific activity and membrane integrity, in addition to the production of intracellular reactive oxygen species (ROS). The effects of the period and dose of exposure were determined by exposing the A549 cell line to various TNT concentrations during different incubation periods.

2.0 Methods

2.1 TNT preparation and characterisation

TNTs were produced using the rapid and low-cost anodization process *via* the anodic oxidation of titanium foil in an aqueous chloride-ion containing electrolyte, as reported in previous publications. (Garvey et al. 2016; Panaitescu et al. 2008; Richter et al. 2007) Briefly, 0.89mm sheets of titanium foil (Alfa Aesar, purity 99.7%) were anodized at 13V DC, using a two-electrode configuration, in a 0.1M ammonium chloride electrolyte solution. A pH of 1.8–2 was upheld by the addition of hydrochloric acid (Alfa Aesar, reagent grade). Well-aligned arrays of TNTs continually formed in corrosion pits, at the surface of the foil. TNTs were subsequently released into the electrolyte solution before forming a precipitate at the bottom of the vessel. The precipitate was collected and washed with water and isopropanol before drying and sieving to remove large agglomerates. The final product formed a white coloured powder, each micron-sized grain of powder comprised a bundle of nanotubes. in a tube furnace at 200, 400, 600 and 800°C respectively using a ramp rate of 10°C/min, a hold time of 1h and

a cooling rate of 10°C/min until room temperature was reached. The nanotubular TiO_2 materials are, herein, referred to as UN TNTs (untreated nanotubes), TNT200, TNT400, TNT600 and TNT800 (NTs annealed at 200, 400, 600 and 800°C respectively). The chemical and textural properties of the UN and annealed TNTs were examined using Scanning electron microscopy (SEM), X-Ray Diffraction, Raman, X-ray photoelectron (XPS) and N_2 gas adsorption studies, as previously described by this group (Garvey et al., 2016) before successive assessment of the cytotoxic effects of the materials. Additionally, a Perkin Elmer Spectrum 100 FTIR spectrometer was used for comprehension of the chemical composition of the Titania nanotube samples. XPS was conducted using a Thermo VG Scientific (East Grinstead, UK) ESCALAB Mk II spectrometer, with an XR3 twin anode X-ray source (AlKα/MgKα) and an Alpha 110 analyser. The twin anode AlKα X-ray source (hn = 1486.6eV) was used at 300W (15 kV x 20 mA) for the analysis of all TNTs. A Pass Energy of 200eV and a step size of 0.4eV were used for all survey spectra. C1s, O1s, Cl2p and Ti2p high resolution spectra were acquired using a Pass Energy of 20 eV and a step size of 0.2 eV. The specific surface areas and pore size distributions of the nanotubes were calculated by the BET (Brunauer–Emmett–Teller) method with the use of a Gemini VII 2390 Surface Area Analyser (Micrometrics) as per Garvey et al., 2016.

2.2 Cell Culture and maintenance

Human A549 lung carcinoma cells (ATCC ACL-185) were grown with continuous sub-culturing in F-12 Nutrient Mix 1x media (Life Technologies™, Gibco®, UK) with 10% foetal bovine serum (FBS) supplemented L-Glutamine and 1% penicillin/streptomycin (P/S). The cell line was maintained in a T75cm^2 cell culture flask (Sarstedt, Germany), within a humidified incubator containing 5% (vol/vol) CO_2, at 37˚C. Sub-culturing was performed every 2-3 days or until 80-90% confluency was reached, *via* the transfer of 200ul of trypsinized cells and the

addition of 15ml fresh media to a new T75cm^2 cell culture flask. Once confluent, cells were aseptically washed with phosphate buffered saline (PBS) and trypsinized, to detach adherent cells. Prior to each cytotoxicity assay, a cell count was performed using a haemocytometer, and cells were seeded in 96-well culture plates and/or 24-well plates, at the specific cell density required by each assay.

2.3 *In vitro* cytotoxicity assessment

2.3.1 Preparation of UN and annealed TNT exposure dispersions

A549 human lung carcinoma cells were exposed to pre-prepared aqueous dispersions of UN and annealed TNTs amid a range of exposure doses (0.8, 1.6 and 2mg/ml), as per the guidelines of each assay kit. At initial exposure doses cytotoxic effects could not be detected using the Clonogenic and ROS assays. Subsequently, these assays were evaluated using exposure doses of 0.04, 0.08 and 0.1mg/ml. The influence of thermal processing on the *in vitro* pulmonary toxicity of TNTs were then assessed using a battery of well-established colorimetric and non-colorimetric cytotoxicity assays including the MTT; Clonogenic; LDH and ROS assays.

2.3.2 MTT assay

The MTT assay (1-(4, 5-Dimethylthiazol-2-yl)-3, 5-diphenylformazan, Thiazolyl blue formazan) is a colorimetric assay, used to assess cellular viability and proliferation. This assay measures the activity of viable mitochondria by monitoring the reduction of yellow tetrazolium salts *via* cellular mitochondrial dehydrogenase enzymes, which produces purple, insoluble formazan dye. The amount of formazan dye formed corresponds to the number of viable cells. The assay was performed as per MTT assay Kit supplied protocol. A 96-well plate was seeded with a cell density of 1.5x10^5 cells/well contained in media supplemented with 10% FBS, and incubating (5% CO_2) for 24h , at 37˚C. A 0.5mg/ml MTT solution (Sigma Aldrich, Ireland)

was prepared in sterile PBS, filtered with a 0.2μm filter to avoid contamination, and stored in the dark at 4-6°C. Cells were then exposed, in replicate, to 0.8, 1.6 and 2mg/ml of the UN and annealed TNTs for 24h at 37˚C. Subsequently, 10μl of MTT solution was added to the exposed cells and incubated (5% CO_2) for a further 4h at 37°C. After this incubation period, a water-insoluble formazan dye is formed. The formazan crystals are solubilized in dimethyl sulfoxide (DMSO) (Sigma-Aldrich Ireland Ltd) and quantitated using a scanning multi-well spectrophotometer (Fluostar Optima BMG Labtech, Ortenberg, Germany), at a wavelength of 595nm. The measured absorbance is proportional to the number of viable cells. Results are presented as percentage of untreated control against the TNT treated cells at different concentrations.

2.3.3 Clonogenic assay

The clonogenic assay monitored the cellular viability of A549 lung cells during a 24h period of exposure to the UN and annealed TNTs. A 24-well plate was seeded with 1ml of $1x10^5$ cells/well contained in media, supplemented with 10% FBS and incubated (5% CO_2) for 24h, at 37˚C. The, media was subsequently removed from the cells, which were then aseptically washed with PBS. The cells were then exposed to 1ml of media, supplemented with 10% FBS that contained 0.04, 0.08 and 0.1mg/ml of the UN and annealed TNTs and incubated (5% CO_2) for a further 24h, at 37˚C. Following incubation, cells were detached from the 24-well plates using 250μl of trypsin and a 15-minute incubation (5% CO_2, 37˚C). Finally, the A549 lung cells were stained with trypan blue, in a 1:1 cell to trypan blue ratio, and a viable cell count was recorded. Results are presented as percentage of untreated control against the TNT treated cells at different concentrations.

2.3.4 LDH

The LDH Cytotoxicity Assay Kit (Thermo Scientific™) is a colorimetric assay which measures the quantity of lactate dehydrogenase (LDH) produced by cells. The release of LDH, is a cytosolic enzyme present in many cell types, into cell media is an indication of cellular membrane damage. This assay was performed as per LDH Cytotoxicity Assay Kit (Thermo Scientific™) supplied protocol. A 96-well plate was seeded with 100µl of $1x10^5$ cells/well contained in media, supplemented with 10% FBS and incubated (5% CO_2) for 24h, at 37˚C. The, media was subsequently removed from the cells and replaced with new media that contained 0.8, 1.6 and 2mg/ml of the UN and annealed TNTs, before incubating (5% CO_2) for 24h, at 37˚C. Following incubation, the amount of lactate dehydrogenase produced was quantitated using a scanning multi-well spectrophotometer (Fluostar Optima BMG Labtech, Ortenberg, Germany), at wavelengths of 490nm and 680nm. Results are presented as percentage of untreated control against the TNT treated cells at different concentrations.

2.3.5 Reactive Oxygen Species (ROS) assay

The Cellular Reactive Oxygen Species Detection Assay Kit (Red Fluorescence) (abcam™) is used to measure the extent of cellular ROS generation. ROS are natural by-products of cellular metabolic activity. However, oxidative stress reflects a bodily free radicals and antioxidants and is often associated with a dramatic increase in ROS levels. The accumulation of ROS thus indicates cellular damage. This assay was performed as per the Cellular Reactive Oxygen Species Detection Assay Kit (Red Fluorescence) (abcam™) supplied protocol. A 96-well plate was seeded with 100µl of $1x10^5$ cells/well contained in media, supplemented with 10% FBS and incubated (5% CO_2) for 24h, at 37˚C. The, media was subsequently removed from the cells and replaced with new media that contained 0.04, 0.08 and 0.1mg/ml of the UN and annealed TNTs, before incubating (5% CO_2) for 24h, at 37˚C. The assay was then completed as per

Cellular Reactive Oxygen Species Detection Assay Kit instructions. The fluorescence was monitored at Ex/Em=520/605nm using using a scanning multi-well spectrophotometer (Fluostar Optima BMG Labtech, Ortenberg, Germany). Results are presented as percentage of untreated control against the TNT treated cells at different concentrations.

2.3.6 Statistics

All experimental data is an average of 3 experimental replicates with 4 internal replicates per plate. Cytotoxicity induced from test samples was measured as %reduction or proliferation of the untreated control (+/- standard deviation). The control value was taken as 100% viable or 0% toxicity. Student's t-tests and ANOVA one-way model (MINITAB software release 16; Mintab Inc., State College, PA) were used to determine the toxicity of each TNT type at 95% level of confidence ($p<0.05$).

3.0 Results

3.1 Characterization of TNTs

The physiochemical properties, primarily the morphology and crystalline composition of UN and annealed TNTs were modified *via* thermal processing at various temperatures including 200, 400, 600 and 800°C. Before assessing the cytotoxic action of the TNTs, the physiochemical properties of the nanotubular TiO_2 forms were examined using X-ray diffractograms, raman spectra, scanning electron microscopy images and N_2 adsorption isotherms. X-ray diffractograms, Raman spectra, scanning electron microscopy images and N_2 adsorption isotherms that support the discussed physical and textural properties of the UN and annealed TNTs are presented in a previous work by this group. (Garvey et al. 2016) A summary of the previously characterized physical and textural properties of the UN and annealed TNTs is presented in Table 1. Data detailing information retrieved from the X-ray diffractograms and

Raman spectra presented elsewhere, are summarized in Table 1. (Garvey et al. 2016) The Spurr equation (F_R= 1/1+0.8(I_A(101)/I_R(111)) was also previously applied to determine the anatase and rutile phase content of the TNTs, which have been reported in Table 1. (Garvey et al. 2016) In addition, the Scherer equation ($D = K\lambda/\beta\cos\theta$) was used to determine the particle size of the TNTs (Table 1). (Dervin et al. 2018) The UN TNTs, and TNT200 exhibited a pattern characteristic of amorphous structures. That is, only reflections from the titanium support are visible. [24-27] Generally, untreated anodically grown TNTs are amorphous, transforming to the anatase crystallite phase at ~280°C. (Grimes and Mor 2009; Mohamed et al. 2017; Paulose et al. 2006; Ruan et al. 2005; Varghese et al. 2003) After annealing at a temperature of 400°C, the amorphous TNTs converted to crystalline structures and produced an XRD pattern characteristic of anatase, rutile and anatase/ rutile mixed phase TiO_2 (Table 1). (Garvey et al. 2016) As the treatment succeeded 400°C, the relative intensity of the rutile 110 peak with respect to the anatase 101 peak increased; evident in the XRD patterns shown elsewhere. (Garvey et al. 2016) The anatase content of the TNTs reduced from 86.44% in TNT400 to 33.5% in TNT600 and the TNTs fully converted to rutile at 800°C (Table 1). (Garvey et al. 2016) The variation in crystallite size, associated with the thermal processing temperature is displayed in Table 1. The UN TNTs presented a crystallite size of 4.4-4.7nm. Upon increase in treatment temperature the crystallite size of TNTs also increased to 7.8nm. At 400°C, the walls of the TNTs began to collapse, and anatase crystallites (13nm) begin to grow among the inner walls of the nanotubular structures. Annealing at increased temperatures reduces the average size of the anatase crystallites and facilitates the formation of rutile crystals, and a progressive increase in crystallite size (~34.1nm) (Table 1). The Raman spectra of the TNTs were consistent with the previously presented XRD data, further confirming the impact of annealing on TNT phase content. (Garvey et al. 2016)

Table 1 A summary of the physical and textural properties of the UN and annealed TNTs, previously characterized by this group. ***(Garvey et al. 2016)***

	UN	**200**	**400**	**600**	**800**
Crystallinity	Amorphous /partially crystalline	Amorphous /partially crystalline	Anatase: Rutile 86.44%:13.56%	Rutile: Anatase 66.5%:33.5%	Rutile 100%
Morphology	Nanotubular	Nanotubular	Fragmented Nanotube (Crystalline anatase growth on tube wall)	Fragmented Nanotube (Crystalline anatase growth on tube wall)	Agglomerates of large crystal
Crystalline Size (nm)	4.4-4.7	7.8	Anatase:13 Rutile: -	Anatase:21.5 Rutile:26.6	Rutile:34.1
Particle Size (nm)	Diameter:20 Wall thickness:2–5	Diameter:20 Wall thickness:2–5	5-10	20-30	200-500
Surface area (m^2/g)	55	63	55	10	1
Pore volume (cm^3/g)	0.08	0.08	0.11	0.02	0.002
Pore Diameter (nm)	3.5	3.8	5.6	4.6	4.6

SEM images indicate that thermal processing did not generate any discernible macroscopic or microscopic changes in the UN and annealed TNT. However, high resolution SEM images

presented in a previous study conducted by this group, reveal that several nanoscopic changes occurred due to elevation in treatment temperature. (Garvey et al. 2016) Annealing at 200°C did not considerably alter the amorphous morphology of the TNTs, 20nm in diameter with a wall thickness of 2–5nm. Between 200 and 400°C the TNTs crystallize, forming an anatase rich, mixed phase composition, also confirmed by XRD. The TNT walls also begin to crumble and small anatase crystallite, 5–10nm in size, begin to grow along the tube walls. The size of the anatase crystallites increases to 20–30nm, and the walls of the TNTs further divide as the annealing temperature is increased to 600°C. As the temperature reaches 800°C, the once well aligned bundle of TNTs has completely transformed into an agglomerated arrangement of large crystal

TNSs aligned along the original direction of the former, and rutile crystallite size reaches 200–500nm. (Garvey et al. 2016)

According to the IUPAC, the isotherms of the UN and annealed TNTs, previously published by this group, (Garvey et al. 2016) exhibit a type II pattern characteristic of low-porosity materials or materials containing mesopores. (Sing 1985) The UN TNTs presented a surface area of $55 m^2/g$. As the treatment temperature increased to 200°C the specific surface area was enlarged, reaching $63 m^2/g$, due to crystallization and anatase formation (Table 1). (Garvey et al. 2016) However, the surface area began to decrease once again upon further increase of treatment temperature and corresponding growth of the rutile phase (Table 1). (Garvey et al. 2016) The surface area of TNTs typically reduces as annealing temperature is increased, due to the rearrangement of the crystal structure. (Ou and Lo 2007; Tilly et al. 2014) The pore volume and diameter also increased as the treatment temperature reached 400°C, creating the largest pore volume ($0.112 cm^3/g$) and diameter (5.62nm). The high surface area and large pore volume of TNT400 are ascribed to the formation of mesopores, resulting from densification of amorphous TiO_2 to crystallized TiO_2 during annealed, in addition to the superior anatase

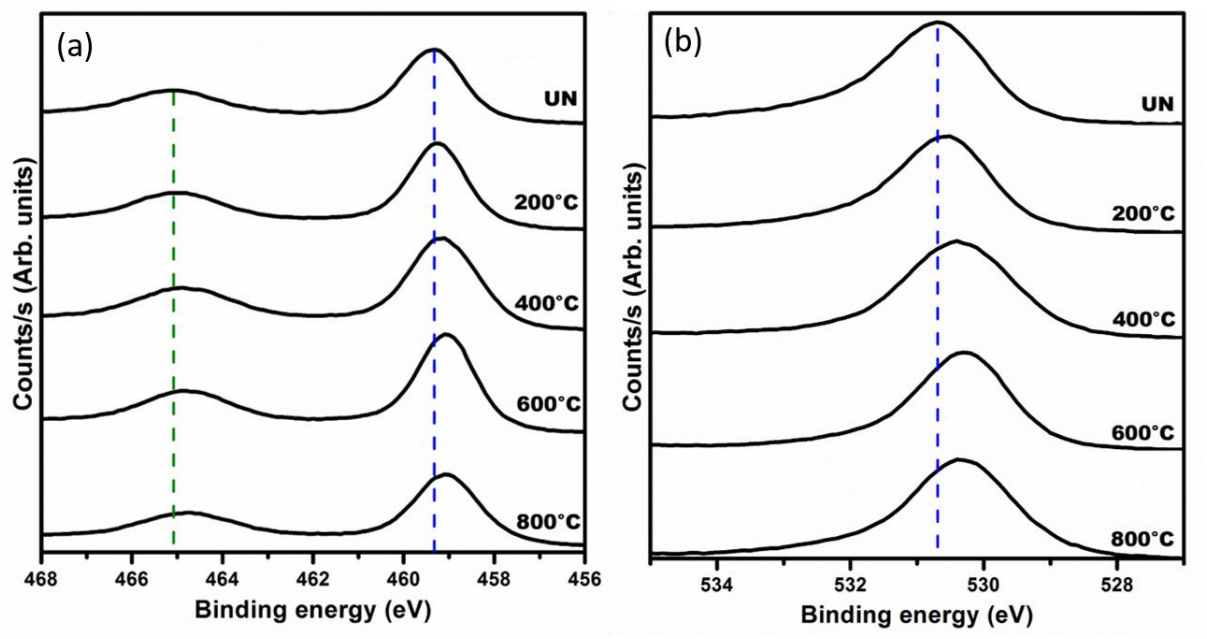

Figure 1 Chemical properties of UN TNTS and TNTS treated at 200, 400, 600 and 800°C: (a) FTIR, (b) High resolution Ti2p XPS spectra, (c) High resolution O1s XPS spectra

Table 2 XPS binding energies of UN and TNTS treated at 200, 400, 600 and 800°C

	C_{1s}	O_{1s}	Ti_{2p}	Cl_{2p}
UN	284.98	530.70	459.33	199.01
200°C	284.97	530.58	459.23	198.76
400°C	284.91	530.37	459.12	198.61
600°C	284.93	530.28	459.05	198.58
800°C	285.08	530.32	459.05	198.73

content. (Zhang et al. 2017) The textural properties of the TNTs began to progressively diminish as the treatment temperature reached 800°C (Table 1).

The FTIR spectrum (500–4000cm^{-1}) of the UN and annealed TNTs is presented in Figure S1 (a). Figure S1 (b) presents the spectra of TNTs recorded in the wavelength range 450–700cm^{-1}. No significant variations in TNT chemical composition were observed, though spectra indicate that the interaction between Ti ions and molecular water reduced as treatment temperature

increased. The presented spectra display weak features characteristic of the TiO_2 skeletal; Ti–O and Ti–O–Ti framework bonds (570–430cm^{-1}), asymmetric carboxylate vibrations (~1550cm^{-1}) and an OH stretch at ~2800-3500 cm^{-1}. (Byrne et al. 2016; Erdem et al. 2001; Kumar et al. 2000; Nolan et al. 2009)

The oxidation state and chemical nature of the UN and annealed TNTs were confirmed using XPS. The TNTS are primarily comprised of titanium and oxygen, also containing synthetic residual chlorine. The binding energies of elements present on the surface of the UN and annealed TNTs are displayed in Table 2. The high resolution XPS scan of the Ti2p region presented in Figure 1 (a), reveals the presence of the main doublet containing two symmetrical peaks centred at approx. 459eV (Ti 2p3/2) and 465eV (Ti2p1/2), depicting Ti^{4+} in a tetragonal structure. (Etacheri et al. 2011; Fahim and Sekino 2009; Rahna et al. 2016) High-resolution O1s spectra of the TNTs are displayed in Figure 1(b). The primary peak at 530 eV can be attributed to O-Ti-O type bonding.(Fahim and Sekino 2009; Jagadale et al. 2008; Rahna et al. 2016) There are slight variations in the binding energy for O_{1s} but there is no indication of oxygen vacancies formation, which is expected with the increase in temperature.(Berger et al. 1993; Dvoranová et al. 2002; Etacheri et al. 2011)

3.2 *In vitro* cytotoxicity assessment of TNTs

3.2.1 Effects of TNT exposure on cell viability

The MTT assay facilitated concurrent examination of the proliferative effects of TNTs and their impact on essential cellular metabolic activity. (Magrez et al. 2009) As can been seen in figure 2, at an exposure dose of 0.8mg/ml the UN TNTs, TNT200 and TNT800 exhibited 76% toxicity. TNT400 and TNT600 demonstrated heightened toxicity of 89 and 85% respectively, at 0.8mg/ml. Initially, the *in vitro* pulmonary toxicity of the UN and annealed TNTs increased as changes in TNT morphology and phase composition began to develop. A processing

temperature of 400°C generated small, anatase rich, fragmented, TNTs (TNT400). According to the MTT assay, TNT400 also exerted the greatest extent of *in vitro* pulmonary toxicity. Elevated annealing temperatures induced a further collapse of the tubular structure, growth and domination of the rutile phase and a reduction in cytotoxic action. Overall however, crystalline TNTs induced a greater degree of toxicity than that of amorphous TNTs. Interestingly, the cytotoxic action of TNTs significantly decreased as the exposure dose of the amorphous and structurally intact TNTs (UN TNT and TNT200) increased. The toxicity exerted by the fragmented, crystalline TNTs (TNT400 and TNT600) and agglomerated TNSs (TNT800) also reduced as exposure dose increased, but to a far lesser extent than the former. This unusual outcome is likely due to nanomaterial interference with the dye of the colorimetric assay. (Dervin et al. 2018) The MTT assay has recently been regarded as being prone to experimental artefacts.(Dervin et al. 2018; Magrez et al. 2009; Wörle-Knirsch et al. 2006) Consequently, toxic responses witnessed from the MTT assay were verified using a range of additional cytotoxic tests.

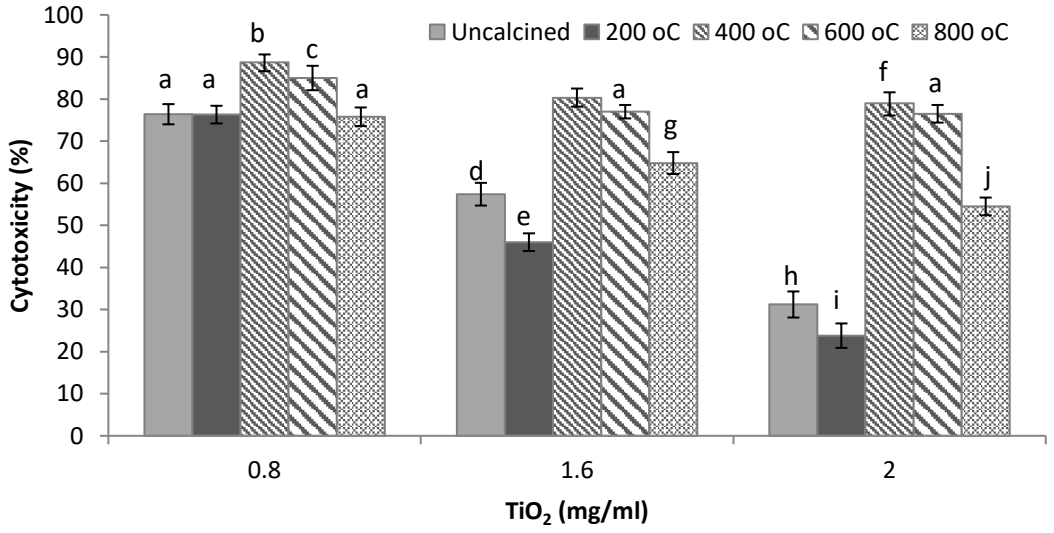

Figure 2 Cytotoxicity (percent of untreated control) of A549 lung cells following exposure to UN and

annealed TNTs (ºC) as determined by the MTT assay (+/-S.D). a, b, c, d, e, f, g, h, i and j denotes significant difference at p<0.05.

To evade experimental artefacts, the clonogenic assay was used to evaluate the effects of TNTs on cell viability *via* direct measurement of cellular growth, avoiding the use of colorimetric endpoints (e.g. MTT and LDH assays). (Monteiro-Riviere et al. 2009; Wörle-Knirsch et al. 2006) In contrast to the MTT assay, a direct measurement of cellular growth after TNT exposure indicated a dose dependent increase in toxicity (Figure 3). At the greatest treatment dose (0.1mg/ml), all TNTs induced a considerable degree of *in vitro* pulmonary toxicity. Untreated, amorphous and intact TNTs (UN TNTs and TNT200) reduced cell survival by 84%. Fragmented, crystalline TNTs (TNT400 and TNT600) and agglomerated rutile TNSs

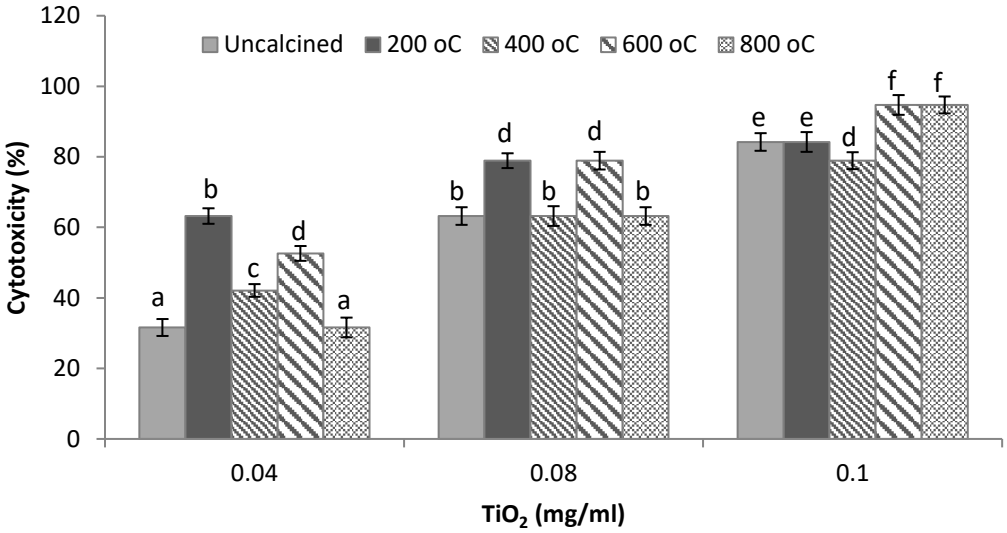

Figure 3 Cytotoxicity (percent of untreated control) of A549 lung cells following exposure to UN and annealed TNTs (ºC) as determined by the clonogenic assay (+/-S.D). a, b, c, d, e and f denote significant difference at p<0.05.

(TNT800) produced toxicities of ≥90%. At milder exposure doses, however, (0.04mg/ml), amorphous TNTs that retained their structure (TNT200) after mild annealing (200^{o}C) induced a greater reduction in cell viability than all other TNTs. The outcome of the clonogenic assay thus suggests that amorphous TNTs, subjected to mild thermal processing (200^{o}C) and mixed

crystalline phase, fragmented TNTs with a rutile rich content exerted the greatest degree of *in vitro* pulmonary toxicity.

3.2.2 Effects of TNT exposure on cell membrane integrity

The LDH assay is implemented to determine the extent of membrane damage upon TNT exposure. (Chan et al. 2013) The assessment of membrane integrity is a customary measure of cell viability and toxic response, and is a required endpoint for measuring the biocompatibility

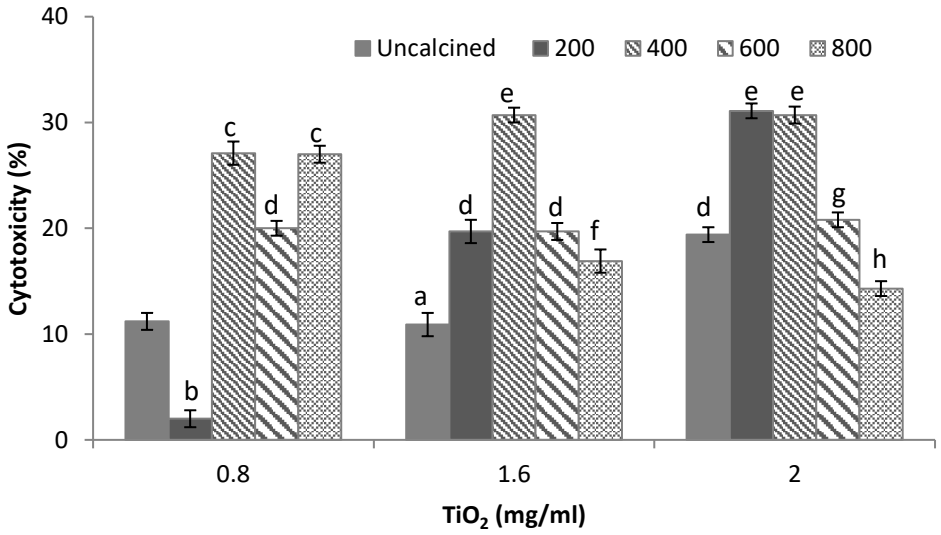

Figure 4 Cytotoxicity (percent of untreated control) of A549 lung cells following exposure to UN and annealed TNTs (ºC) as determined by the LDH assay (+/-S.D). a, b, c, d, e, f, g and h denote significant difference at p<0.05.

of medical devices under the ISO guidelines (Mohamed et al. 2017) All TNTs under study induced mild but noteworthy membrane disruption (<40%). At the lowest exposure dose of 0.8mg/ml, amorphous, intact TNTs (UN TNTs and TNT200) generated the least amount of damage (≥10%). At a maximum exposure dose of 2mg/ml, however, UN TNTs and TNT200 exerted up to a 20% decrease in viability (Figure 4). Fragmented TNTs (TNT400 and TNT600) and agglomerated rutile TNSs (TNT800) generally induced a greater loss in viability than

nanotubular structures. At a maximum treatment dose however, the greatest membrane damage (~31%) resulted from exposure to TNT200 and TNT400, indicating that intact TNTs of mixed phase composition, with an anatase rich content (86.44%:13.56% anatase: rutile mixed phase) and small particle and crystallite size were most capable of physical cellular disruption. As treatment temperature increased to 600 and 800^{o}C, the anatase content of TNTs diminished (Figure 1), crystallite and particle size increased, and lesser membrane damage was observed (Figure 4). Furthermore, in correlation with the clonogenic assay the, the LDH assay indicates TNT toxicity is dose dependent.

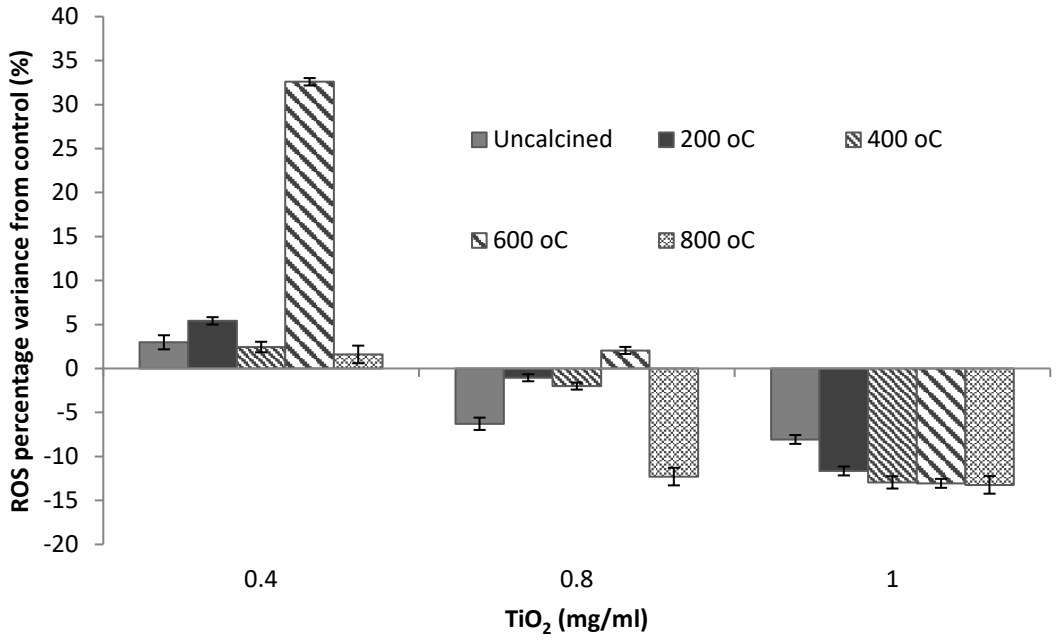

Figure 5 Variance in levels of reactive oxygen species present with varying concentrations of UN annealed TNTs (^{o}C) as determined by the ROS kit. ROS is calculated as a percentage decrease or increase compared to the untreated control taken as 100%.

3.2.3 Effects of TNT exposure on intracellular ROS production

An increased production of intracellular reactive oxygen species (ROS) is an imperative measure of nanotoxicity.(Colvin 2003; Nel et al. 2006; Patravale et al. 2012; Xia et al. 2008) The physiochemical characteristics of many metal oxide nanoforms, including lateral dimensions and structural morphology, surface area, chemical composition, oxidation state and

surface species, often stimulate inflammation. This toxic response enhances the conversion of less toxic oxidants into more reactive oxygen species, responsible for inducing oxidative stress, DNA damage, disordered cell signalling, and subsequent changes in cell motility and survival. (Fu et al. 2014; Lu et al. 2010; Ray et al. 2009; Wang et al. 2008) However previously published studies have asserted that titania induced toxicity is not mediated by ROS generation. (Xia et al. 2008) The current assessment of ROS activity suggested that ROS mediated oxidative stress was not the predominant mode of TNT cytotoxic action (Figure 8). For the most part, TNTs acted as an ROS suppressor (Figure 8). The lowest treatment dose of all TNTs exposed to A549 lung cells, 0.4mg/ml, stimulated an increased production of ROS, with TNT600 generating a maximal 35% increase. As the treatment dose increased to 0.8 mg/ml all TNTs, other than those treated at 600^{o}C caused a reduction in the quantity of ROS present compared to the untreated control. TNT600 generated a 4% increase in ROS production, though this decreased as exposure dose increased (Figure 8). An increase in TNT concentration to 1 mg/ml suppressed ROS production by up to 13%.

3.3 Discussion

The impressive advancement of nanotechnology engenders growing concern for the classification of nanomaterial toxicity. Though researched for decades, the biocompatibility of nanoscale titania is still under careful scrutiny. Exposure to TNTs occurs at an industrial scale, during production, subsequent formulation and product development. Also at a research scale, with inhalation regarded as a primary route of TNT exposure in the workplace. (Shi et al. 2013) Modification of TNTs due to post-synthetic processing, for product manufacture and design, alters the biocompatibility of these materials further; an apprehension not often deliberated during industrial production or *in vitro* toxicity assessments, a common first step in the evaluation of health hazards relating to engineered nanomaterials. (Drasler et al. 2017)

Accordingly, this study assessed the *in vitro* pulmonary toxicity of TNTs induced by morphological and crystalline changes associated with post-synthetic thermal processing.

A549 lung carcinoma cells were exposed to untreated, amorphous TNTs and those treated at 200, 400, 600 and 800^{o}C, respectively. The cytotoxic action of the untreated and annealed TNTs was assessed using a battery of cytotoxicity assays that examined cellular metabolic and prolific activity and membrane integrity, in addition to the production of intracellular reactive oxygen species (ROS). The effects of the period and dose of exposure were determined by exposing the A549 cell line to various TNT concentrations during different incubation periods. The untreated and annealed TNTs elicited an overall dose dependent increase in toxicity. As the annealing temperature increased from 200-800^{o}C the nanotubular structure of TNTs diminished and changes in crystalline phase composition developed. Crystalline nanoparticles also began to grow among the dividing walls of the TNTs, and the crystallite and particle size increased progressively. Irrespective of processing conditions, the untreated and annealed TNTs exerted significant *in vitro* pulmonary toxicity. Adjusting the treatment during thermal processing also results in varied degrees of cytotoxic action. Thus, the deviation in TNT biocompatibility as a result of post-synthetic processing is illustrated. Furthermore, it is evident that a specific property alone does not dictate toxicity. Rather, a synergistic relationship of specific nanomaterial properties manifests various degrees of toxicity.

3.3.1 Effects of UN and annealed TNT crystallinity on the A549 alveolar cell line

Crystallinity has previously been suggested to influence the toxic potential of TNMs. (Johnston et al. 2009)

Generally, anatase TNMs are considered more toxic than those of rutile orientation. (De Matteis et al. 2016) The enhanced reactivity of the anatase Titania form has been considered to provoke greater inflammatory effects by ROS generation, subsequent oxidative stress

mediation and DNA damage, than the rutile phase. (De Matteis et al. 2016; Falck et al. 2009; Huerta-García et al. 2014; Petković et al. 2011; Xue et al. 2010) Although hydroxyl radical generation on the surface of TNMs is considered the principal mechanism of Titania toxicity, (Bar-Ilan et al. 2012; George et al. 2011) Gurr and co-workers (Gurr et al. 2005) previously revealed that only rutile TNMs increase the release of hydrogen peroxide if incubated in the dark, not the anatase form. (Gerloff et al. 2012; Xiong et al. 2013) Fenoglio *et. al* later established, however, that anatase or anatase/rutile Titania can mediate direct oxidative damage to organic molecules in the dark *via* an oxygenated free radical dissociated reaction. (Fenoglio et al. 2009) In fact, without UV irradiation, rutile TiO_2 nanoparticles are more photocatalytic than anatase and consequently, are able to generate higher amounts of oxygenated free radicals on their own surface. (Fenoglio et al. 2009; Lipovsky et al. 2012; Uboldi et al. 2016) The MTT and clonogenic assays, indicated that crystallinity is a key factor influencing the toxicity of TNTs. Amorphous TNTs produced significant cytotoxicity, yet exposure to crystalline TNTs created a more damaging impact. Findings of the MTT assay suggest anatase rich, mixed phase, crystalline TNTs have the greatest tendency to induce toxicity, followed by rutile rich, mixed phase crystalline TNTs and agglomerated rutile TNSs, respectively. The clonogenic assay, however, attests that rutile rich, mixed phase, crystalline TNTs are more toxic, at increased exposure doses, than anatase rich TNTs. Interpretation of A549 membrane damage also emphasizes the role of crystallinity in TNT toxicity. At low exposure doses, amorphous TNTs substantiated the least membrane damage and consequential LDH leakage. Fragmented, crystalline TNTs and agglomerated rutile TNSs produced a toxic response, in excess of 90%. However, at milder exposure doses TNTs influenced more significant disruption. The toxicity of mixed phase crystalline TNTs may be related to a synergic effect dictated by the coexistence of similarly sized anatase and rutile aggregates (Table 1), rather than the mere emergence of the rutile phase.(Deiana et al. 2010; Gerloff et al. 2012; Ohno et al. 2001)

3.3.2 Effects of UN and annealed TNTs size and shape on the A549 alveolar cell line

Size and shape are considered the most likely attributes of nanotoxicity. (Fu et al. 2014) Watari *et al*. systematically investigated the size effect of titania on cell toxicity, revealing nanomaterials >3µm were easily internalized through the respiratory system. In accordance with the findings of Watari *et al*. The MTT and LDH viability measures suggests that anatase containing TNTs of smallest crystallite and particle size (TNT400) prompted heightened levels of toxicity. The clonogenic assay indicated that mixed phase, rutile rich TNTs, with a larger crystallite size, in addition to agglomerated rutile TNSs induce a more pronounced decrease in cell viability. Although stronger effects were expected from exposure to TNTs of smaller particle size, (Johnston et al. 2009) the larger particle induced toxicity may be governed by state of agglomeration. Numerous nanotoxicity evaluations have considered the role of aggregation/agglomeration, several investigations have highlighted the dictating influence of agglomeration on NM uptake, though responses vary throughout diverging cell lines. (Hirsch et al. 2013; Murdock et al. 2008; Okuda-Shimazaki et al. 2010; Safi et al. 2010) Furthermore, the MTT and LDH assays indicated fragmented TNTs are the most toxic class of structure assessed, at minimum exposure doses. Clonogenic measurements dispute this assertion, alleging that, at minimal exposure doses, intact TNTs are most toxic. As exposure dose increases however, findings of the aforementioned assays are in correlation with one another, indicating that a disintegrated tubular shape produces greater or comparable levels of toxicity, than an intact TNT.

3.3.3 Effects of UN and annealed TNT surface area on the A549 alveolar cell line

Surface area has been established as another central parameter influencing TNM toxicity. (Nel et al. 2006; Oberdörster et al. 2005a; Oberdörster et al. 2005b; Xiong et al. 2013) The surface

area regulates the reactivity of nanostructure surfaces, thus large surface area, in conjunction with small particle size and the ability to generate ROS have previously been reported to determine the toxic potential of TNMs. (Donaldson et al. 2004; Donaldson and Tran 2002; Gerloff et al. 2012; Nel 2005; Nel et al. 2006; Xiong et al. 2013) However, particle aggregation can modify the effects of particle size. It is therefore also possible for nanomaterialss to induce toxicity in an aggregated state. (Nel et al. 2006) The findings presented within do not evidence a correlation between toxicity and TNT surface area.

3.3.4 UN and annealed TNTs repress ROS generation

ROS mediated oxidative stress elicits acute protein and DNA damage, disrupting customary cellular responses, due to the existence of surface radicals or *via* NM and cellular component interactions. (Dreher 2004; Fröhlich 2012; Ma et al. 2017; Singh et al. 2007; Xia et al. 2006) Published literature has accentuated the role of TNMs in ROS generation and subsequent cellular oxidative stress, having identified this mechanism as a primary factor inducing TNM toxicity. (De Matteis et al. 2016; Donaldson et al. 2005; Gali et al. 2016; Gerloff et al. 2012; Huang et al. 2014; Hussain et al. 2010; Mohamed et al. 2017; Oberdörster et al. 2005b; Shi et al. 2013; Tsaryk et al. 2013; Zhu et al. 2012) Remarkably, the reduction in cell viability and membrane damage, induced by intact, amorphous TNTs, fragmented, crystalline TNTs and agglomerated rutile TNSs, could not be explained by discernible oxidative stress generation. Irrespective of post-synthetic processing conditions, all TNTs repressed ROS production at the highest exposure dose (1mg/ml). Due to the physicochemical properties associated with TNTs, including chemical composition, surface area, their relatively low solubility and their ability to catalyse ROS production (Manke et al. 2013), the cytotoxic potential of these robust materials is expected to be mostly propelled by oxidative stress. [31] The studies described herein suggest

that this may not be the case, as alternative mechanisms of toxicity are evident for the TNTs under investigation.

3.3.5 UN and annealed TNT assay impedance

The primary properties of nanomaterials, including large, chemically active surface areas, often entices viability assay impedance. The MTT and LDH assays, have recently yielded inaccurate assessment of toxicities, ultimately averting the procurement of comparable toxicity data. (Holder et al. 2012; Kroll et al. 2012; Liang et al. 2015; Ong et al. 2014) In order to evade inconsistent accounts, of varying toxicity exhibited by equivalent nanomaterials, standardized nanotoxicity screening protocols are required. The clonogenic assay facilitates an accurate, highly sensitive and valuable measure of toxicity. (Herzog et al. 2007) The established credibility of the clonogenic assay, resulted in prime dependence on the latter when constructing a potential mechanism of toxicity for the examined TNTs. The clonogenic assay indicated that that amorphous TNTs, subjected to mild thermal processing (200^{o}C) and mixed crystalline phase, fragmented TNTs with a rutile rich content exerted the greatest degree of *in vitro* pulmonary toxicity. The degree of toxicity is influenced by both TNT morphology and phase composition. The exact route of toxicity requires further investigation, but physical membrane damage presumably associated with the modified nanotubular structures, plays an apparent role. Nonetheless, post-synthetic processing creates an additional risk to those exposed in the workplace. The physiochemical modification of nanomaterials, during post-synthetic manufacturing processes requires constant consideration both at an industrial and research scale.

4. 0 Conclusion

Exposure of A549 lung epithelial cells to TNTs, irrespective of dimensionality or crystallinity elicited an overall dose dependent toxic response *in vitro*. Post-synthetic manufacturing processes such as thermal annealing expose new risks of undetermined toxicity to individuals in the workplace. The current assessment illustrates that annealing at elevated temperatures beyond 200^{o}C alters the biocompatibility of TNTs, intensifying the toxic impact of the reformed TNT structures. As treatment temperature increased the nanotubular structure of TNTs fragmented and crystallized, crystal growth was witnessed amongst the dividing, inner TNT walls, and crystallite and particle size increased progressively. The increase in size of the TNTs and domination of a more rigid, rutile phase induced greater loss in viability, as opposed to the levels of toxicity caused by amorphous TNTs and smaller, mixed phase, crystalline TNTs with an anatase rich content.

Author contributions

The manuscript was written through contributions of all authors. All authors have given approval to the final version of the manuscript.

Acknowledgments

Saoirse Dervin wishes to acknowledge the Institute of Technology Sligo for providing financial Support.

References

Albu SP et al. (2008) Formation of Double-Walled TiO2 Nanotubes and Robust Anatase Membranes Advanced Materials 20:4135-4139 doi:10.1002/adma.200801189

AlHoshan MS, BaQais AA, Al-Hazza MI, Al-Mayouf AM (2012) Heat treatment and electrochemical activation of titanium oxide nanotubes: The effect of hydrogen doping on electrochemical behavior Electrochimica Acta 62:390-395 doi:https://doi.org/10.1016/j.electacta.2011.12.048

Bai Y, Mora-Sero I, De Angelis F, Bisquert J, Wang P (2014) Titanium dioxide nanomaterials for photovoltaic applications Chemical reviews 114:10095-10130

Baiju KV, Shukla S, Biju S, Reddy MLP, Warrier KGK (2009) Hydrothermal processing of dye-adsorbing one-dimensional hydrogen titanate Materials Letters 63:923-926 doi:https://doi.org/10.1016/j.matlet.2009.01.041

Balaur E, Macak JM, Tsuchiya H, Schmuki P (2005) Wetting behaviour of layers of TiO2 nanotubes with different diameters Journal of Materials Chemistry 15:4488-4491 doi:10.1039/B509672C

Bar-Ilan O, Louis KM, Yang SP, Pedersen JA, Hamers RJ, Peterson RE, Heideman W (2012) Titanium dioxide nanoparticles produce phototoxicity in the developing zebrafish Nanotoxicology 6:670-679

Berger H, Tang H, Lévy F (1993) Growth and Raman spectroscopic characterization of TiO 2 anatase single crystals Journal of crystal growth 130:108-112

Bhosle SM, Friedrich CR (2017) Rapid heat treatment for anatase conversion of titania nanotube orthopedic surfaces Nanotechnology 28:405603 doi:10.1088/1361-6528/aa8399

Brahmi H, Katwal G, Khodadadi M, Chen S, Paulose M, Varghese OK, Mavrokefalos A (2015) Thermalâ??structural relationship of individual titania nanotubes Nanoscale 7:19004-19011 doi:10.1039/C5NR05072C

Byrne C, Fagan R, Hinder S, McCormack DE, Pillai SC (2016) New approach of modifying the anatase to rutile transition temperature in TiO 2 photocatalysts RSC Advances 6:95232-95238

Byrne C, Subramanian G, Pillai SC (2018) Recent advances in photocatalysis for environmental applications Journal of environmental chemical engineering 6:3531-3555

Camposeco R, Castillo S, Navarrete J, Gomez R (2016) Synthesis, characterization and photocatalytic activity of TiO2 nanostructures: nanotubes, nanofibers, nanowires and nanoparticles Catalysis Today 266:90-101

Chan FK-M, Moriwaki K, De Rosa MJ (2013) Detection of necrosis by release of lactate dehydrogenase activity. In: Immune Homeostasis. Springer, pp 65-70

Chen X, Mao SS (2007) Titanium dioxide nanomaterials: synthesis, properties, modifications, and applications Chem Rev 107:2891-2959

Chen X, Selloni A (2014) Introduction: titanium dioxide (TiO2) nanomaterials. ACS Publications,

Chimene D, Alge DL, Gaharwar AK (2015) Two-dimensional nanomaterials for biomedical applications: emerging trends and future prospects Advanced materials 27:7261-7284

Colvin VL (2003) The potential environmental impact of engineered nanomaterials Nature biotechnology 21:1166

Das K, Bose S, Bandyopadhyay A (2009) TiO2 nanotubes on Ti: Influence of nanoscale morphology on bone cell–materials interaction Journal of Biomedical Materials Research Part A 90A:225-237 doi:10.1002/jbm.a.32088

De Matteis V, Cascione M, Brunetti V, Toma CC, Rinaldi R (2016) Toxicity assessment of anatase and rutile titanium dioxide nanoparticles: The role of degradation in different pH conditions and light exposure Toxicology in Vitro 37:201-210

Deiana C, Fois E, Coluccia S, Martra G (2010) Surface structure of TiO2 P25 nanoparticles: Infrared study of hydroxy groups on coordinative defect sites The Journal of Physical Chemistry C 114:21531-21538

Dervin S, Dionysiou DD, Pillai SC (2016) 2D nanostructures for water purification: graphene and beyond Nanoscale doi:10.1039/C6NR04508A
Dervin S, Murphy J, Aviles R, Pillai SC, Garvey M (2018) An in vitro cytotoxicity assessment of graphene nanosheets on alveolar cells Applied Surface Science 434:1274-1284
Donaldson K, Stone V, Tran C, Kreyling W, Borm PJ (2004) Nanotoxicology. BMJ Publishing Group Ltd,
Donaldson K, Tran CL (2002) Inflammation caused by particles and fibers Inhalation toxicology 14:5-27
Donaldson K et al. (2005) Combustion-derived nanoparticles: a review of their toxicology following inhalation exposure Particle and fibre toxicology 2:10
Drasler B, Sayre P, Steinhäuser KG, Petri-Fink A, Rothen-Rutishauser B (2017) In vitro approaches to assess the hazard of nanomaterials NanoImpact 8:99-116
Dreher KL (2004) Health and environmental impact of nanotechnology: toxicological assessment of manufactured nanoparticles Toxicological Sciences 77:3-5
Drobne D (2018) Spotlighting CLH report for TiO2: nano-safety perspective Chemical Engineering Journal
Dvoranová D, Brezová V, Mazúr M, Malati MA (2002) Investigations of metal-doped titanium dioxide photocatalysts Applied Catalysis B, Environmental 37:91-105 doi:10.1016/S0926-3373(01)00335-6
ECHA proposes classification of TiO2 as category 2 carcinogen (2017) Additives for Polymers 2017:9-10 doi:https://doi.org/10.1016/S0306-3747(17)30153-7
Erdem B, Hunsicker RA, Simmons GW, Sudol ED, Dimonie VL, El-Aasser MS (2001) XPS and FTIR surface characterization of TiO2 particles used in polymer encapsulation Langmuir 17:2664-2669
Etacheri V, Seery MK, Hinder SJ, Pillai SC (2011) Oxygen Rich Titania: A Dopant Free, High Temperature Stable, and Visible-Light Active Anatase Photocatalyst Advanced Functional Materials 21:3744-3752
Fahim NF, Sekino T (2009) A novel method for synthesis of titania nanotube powders using rapid breakdown anodization Chemistry of Materials 21:1967-1979
Falck G et al. (2009) Genotoxic effects of nanosized and fine TiO2 Human & experimental toxicology 28:339-352
Fang D, Luo Z, Huang K, Lagoudas DC (2011) Effect of heat treatment on morphology, crystalline structure and photocatalysis properties of TiO 2 nanotubes on Ti substrate and freestanding membrane Applied Surface Science 257:6451-6461
Fenoglio I, Greco G, Livraghi S, Fubini B (2009) Non-UV-induced radical reactions at the surface of TiO2 nanoparticles that may trigger toxic responses Chemistry-A European Journal 15:4614-4621
Fröhlich E (2012) The role of surface charge in cellular uptake and cytotoxicity of medical nanoparticles International journal of nanomedicine 7:5577
Fu PP, Xia Q, Hwang H-M, Ray PC, Yu H (2014) Mechanisms of nanotoxicity: generation of reactive oxygen species Journal of food and drug analysis 22:64-75
Fujishima A, Honda K (1972) Electrochemical photolysis of water at a semiconductor electrode nature 238:37
Gali NK, Ning Z, Daoud W, Brimblecombe P (2016) Investigation on the mechanism of non-photocatalytically TiO2-induced reactive oxygen species and its significance on cell cycle and morphology Journal of Applied Toxicology 36:1355-1363
Ganguly P, Byrne C, Breen A, Pillai SC (2018) Antimicrobial activity of photocatalysts: fundamentals, mechanisms, kinetics and recent advances Applied Catalysis B: Environmental 225:51-75
Garvey M, Panaitescu E, Menon L, Byrne C, Dervin S, Hinder SJ, Pillai SC (2016) Titania nanotube photocatalysts for effectively treating waterborne microbial pathogens Journal of Catalysis 344:631-639 doi:http://dx.doi.org/10.1016/j.jcat.2016.11.004
George S et al. (2011) Role of Fe doping in tuning the band gap of TiO2 for the photo-oxidation-induced cytotoxicity paradigm Journal of the American Chemical Society 133:11270-11278

Gerloff K et al. (2012) Distinctive toxicity of TiO2 rutile/anatase mixed phase nanoparticles on Caco-2 cells Chemical research in toxicology 25:646-655
Ghicov A, Tsuchiya H, Hahn R, Macak JM, Muñoz AG, Schmuki P (2006) TiO2 nanotubes: H+insertion and strong electrochromic effects Electrochemistry Communications 8:528-532 doi:https://doi.org/10.1016/j.elecom.2006.01.015
Ghicov A, Tsuchiya H, Macak JM, Schmuki P (2005) Titanium oxide nanotubes prepared in phosphate electrolytes Electrochemistry Communications 7:505-509 doi:https://doi.org/10.1016/j.elecom.2005.03.007
Grätzel M (2001) Photoelectrochemical cells nature 414:338
Grimes CA, Mor GK (2009) Material properties of TiO2 nanotube arrays: structural, elemental, mechanical, optical and electrical. In: TiO2 Nanotube Arrays. Springer, pp 67-113
Gurr J-R, Wang AS, Chen C-H, Jan K-Y (2005) Ultrafine titanium dioxide particles in the absence of photoactivation can induce oxidative damage to human bronchial epithelial cells Toxicology 213:66-73
Hamilton RF, Wu N, Porter D, Buford M, Wolfarth M, Holian A (2009) Particle length-dependent titanium dioxide nanomaterials toxicity and bioactivity Particle and fibre toxicology 6:35
Henderson MA, Lyubinetsky I (2013) Molecular-level insights into photocatalysis from scanning probe microscopy studies on TiO2 (110) Chemical reviews 113:4428-4455
Hendren CO, Mesnard X, Dröge J, Wiesner MR (2011) Estimating production data for five engineered nanomaterials as a basis for exposure assessment. ACS Publications,
Herzog E, Casey A, Lyng FM, Chambers G, Byrne HJ, Davoren M (2007) A new approach to the toxicity testing of carbon-based nanomaterials—the clonogenic assay Toxicology letters 174:49-60
Hirsch V, Kinnear C, Moniatte M, Rothen-Rutishauser B, Clift MJ, Fink A (2013) Surface charge of polymer coated SPIONs influences the serum protein adsorption, colloidal stability and subsequent cell interaction in vitro Nanoscale 5:3723-3732
Hoet PH, Brüske-Hohlfeld I, Salata OV (2004) Nanoparticles–known and unknown health risks Journal of nanobiotechnology 2:12
Holder AL, Goth-Goldstein R, Lucas D, Koshland CP (2012) Particle-induced artifacts in the MTT and LDH viability assays Chemical research in toxicology 25:1885-1892
Hou J, Wang L, Wang C, Zhang S, Liu H, Li S, Wang X (2018) Toxicity and mechanisms of action of titanium dioxide nanoparticles in living organisms Journal of Environmental Sciences
Hou J, Wang L, Wang C, Zhang S, Liu H, Li S, Wang X (2019) Toxicity and mechanisms of action of titanium dioxide nanoparticles in living organisms Journal of Environmental Sciences 75:40-53 doi:https://doi.org/10.1016/j.jes.2018.06.010
Hoyer P (1996) Formation of a Titanium Dioxide Nanotube Array Langmuir 12:1411-1413 doi:10.1021/la9507803
Huang K-T et al. (2014) Titanium nanoparticle inhalation induces renal fibrosis in mice via an oxidative stress upregulated transforming growth factor-β pathway Chemical research in toxicology 28:354-364
Huerta-García E, Pérez-Arizti JA, Márquez-Ramírez SG, Delgado-Buenrostro NL, Chirino YI, Iglesias GG, López-Marure R (2014) Titanium dioxide nanoparticles induce strong oxidative stress and mitochondrial damage in glial cells Free Radical Biology and Medicine 73:84-94
Hussain S et al. (2010) Carbon black and titanium dioxide nanoparticles elicit distinct apoptotic pathways in bronchial epithelial cells Particle and fibre toxicology 7:10
Jagadale TC, Takale SP, Sonawane RS, Joshi HM, Patil SI, Kale BB, Ogale SB (2008) N-doped TiO2 nanoparticle based visible light photocatalyst by modified peroxide sol− gel method The journal of physical chemistry C 112:14595-14602
Johnston HJ, Hutchison GR, Christensen FM, Peters S, Hankin S, Stone V (2009) Identification of the mechanisms that drive the toxicity of TiO 2 particulates: the contribution of physicochemical characteristics Particle and fibre toxicology 6:33

Jung JH, Kobayashi H, van Bommel KJC, Shinkai S, Shimizu T (2002) Creation of Novel Helical Ribbon and Double-Layered Nanotube TiO2 Structures Using an Organogel Template Chemistry of Materials 14:1445-1447 doi:10.1021/cm011625e

Kaneco S, Shimizu Y, Ohta K, Mizuno T (1998) Photocatalytic reduction of high pressure carbon dioxide using TiO2 powders with a positive hole scavenger Journal of Photochemistry and Photobiology A: Chemistry 115:223-226 doi:https://doi.org/10.1016/S1010-6030(98)00274-3

Kasuga T, Hiramatsu M, Hoson A, Sekino T, Niihara K (1998) Formation of Titanium Oxide Nanotube Langmuir 14:3160-3163 doi:10.1021/la9713816

Kasuga T, Hiramatsu M, Hoson A, Sekino T, Niihara K (1999) Titania Nanotubes Prepared by Chemical Processing Advanced Materials 11:1307-1311 doi:10.1002/(SICI)1521-4095(199910)11:15<1307::AID-ADMA1307>3.0.CO;2-H

Khan A et al. (2017) The role of graphene oxide and graphene oxide-based nanomaterials in the removal of pharmaceuticals from aqueous media: a review Environmental Science and Pollution Research 24:7938-7958

Khan SUM, Al-Shahry M, Ingler WB (2002) Efficient Photochemical Water Splitting by a Chemically Modified n-TiO₂ Science 297:2243-2245 doi:10.1126/science.1075035

Kroll A, Pillukat MH, Hahn D, Schnekenburger J (2012) Interference of engineered nanoparticles with in vitro toxicity assays Archives of toxicology 86:1123-1136

Kuchibhatla SVNT, Karakoti AS, Bera D, Seal S (2007) One dimensional nanostructured materials Progress in Materials Science 52:699-913 doi:https://doi.org/10.1016/j.pmatsci.2006.08.001

Kumar PM, Badrinarayanan S, Sastry M (2000) Nanocrystalline TiO2 studied by optical, FTIR and X-ray photoelectron spectroscopy: correlation to presence of surface states Thin solid films 358:122-130

Lee J-H, Leu I-C, Hsu M-C, Chung Y-W, Hon M-H (2005) Fabrication of Aligned TiO2 One-Dimensional Nanostructured Arrays Using a One-Step Templating Solution Approach The Journal of Physical Chemistry B 109:13056-13059 doi:10.1021/jp052203l

Lee K, Mazare A, Schmuki P (2014) One-dimensional titanium dioxide nanomaterials: nanotubes Chemical reviews 114:9385-9454

Lei Y et al. (2001) Preparation and photoluminescence of highly ordered TiO2 nanowire arrays Applied Physics Letters 78:1125-1127 doi:10.1063/1.1350959

Liang L et al. (2015) Nanoparticles' interference in the evaluation of in vitro toxicity of silver nanoparticles RSC Advances 5:67327-67334

Linsebigler AL, Lu G, Yates Jr JT (1995) Photocatalysis on TiO2 surfaces: principles, mechanisms, and selected results Chemical reviews 95:735-758

Lipovsky A, Tzitrinovich Z, Gedanken A, Lubart R (2012) The different behavior of rutile and anatase nanoparticles in forming oxy radicals upon illumination with visible light: an EPR study Photochemistry and photobiology 88:14-20

Liu Z, Zhang X, Nishimoto S, Murakami T, Fujishima A (2008) Efficient Photocatalytic Degradation of Gaseous Acetaldehyde by Highly Ordered TiO2 Nanotube Arrays Environmental Science & Technology 42:8547-8551 doi:10.1021/es8016842

Lu W, Senapati D, Wang S, Tovmachenko O, Singh AK, Yu H, Ray PC (2010) Effect of surface coating on the toxicity of silver nanomaterials on human skin keratinocytes Chemical physics letters 487:92-96

Ma Y, Guo Y, Wu S, Lv Z, Zhang Q, Ke Y (2017) Titanium dioxide nanoparticles induce size-dependent cytotoxicity and genomic DNA hypomethylation in human respiratory cells RSC Advances 7:23560-23572

Macak JM, Tsuchiya H, Ghicov A, Yasuda K, Hahn R, Bauer S, Schmuki P (2007a) TiO2 nanotubes: Self-organized electrochemical formation, properties and applications Current Opinion in Solid State and Materials Science 11:3-18 doi:https://doi.org/10.1016/j.cossms.2007.08.004

Macak JM, Zlamal M, Krysa J, Schmuki P (2007b) Self-Organized TiO2 Nanotube Layers as Highly Efficient Photocatalysts Small 3:300-304 doi:10.1002/smll.200600426

Magrez A, Horváth L, Smajda R, Salicio V, Pasquier N, Forro L, Schwaller B (2009) Cellular toxicity of TiO2-based nanofilaments Acs Nano 3:2274-2280
Manke A, Wang L, Rojanasakul Y (2013) Mechanisms of nanoparticle-induced oxidative stress and toxicity BioMed research international 2013
Masciangioli T, Zhang W-X (2003) Peer reviewed: environmental technologies at the nanoscale. ACS Publications,
Mohamed MS, Torabi A, Paulose M, Kumar DS, Varghese OK (2017) Anodically Grown Titania Nanotube Induced Cytotoxicity has Genotoxic Origins Scientific Reports 7
Monteiro-Riviere N, Inman A, Zhang L (2009) Limitations and relative utility of screening assays to assess engineered nanoparticle toxicity in a human cell line Toxicology and applied pharmacology 234:222-235
Mor GK, Shankar K, Paulose M, Varghese OK, Grimes CA (2006) Use of highly-ordered TiO2 nanotube arrays in dye-sensitized solar cells Nano letters 6:215-218
Murdock RC, Braydich-Stolle L, Schrand AM, Schlager JJ, Hussain SM (2008) Characterization of nanomaterial dispersion in solution prior to in vitro exposure using dynamic light scattering technique Toxicological sciences 101:239-253
Nasr M, Eid C, Habchi R, Miele P, Bechelany M (2018) Recent progress on titanium dioxide nanomaterials for photocatalytic applications ChemSusChem 11:3023-3047
Nel A (2005) Air pollution-related illness: effects of particles Science 308:804-806
Nel A, Xia T, Mädler L, Li N (2006) Toxic potential of materials at the nanolevel science 311:622-627
Nolan NT, Seery MK, Pillai SC (2009) Spectroscopic investigation of the anatase-to-rutile transformation of sol− gel-synthesized TiO2 photocatalysts The Journal of Physical Chemistry C 113:16151-16157
Oberdörster G et al. (2005a) Principles for characterizing the potential human health effects from exposure to nanomaterials: elements of a screening strategy Particle and fibre toxicology 2:8
Oberdörster G, Oberdörster E, Oberdörster J (2005b) Nanotoxicology: an emerging discipline evolving from studies of ultrafine particles Environmental health perspectives 113:823
Ohno T, Sarukawa K, Tokieda K, Matsumura M (2001) Morphology of a TiO2 photocatalyst (Degussa, P-25) consisting of anatase and rutile crystalline phases Journal of Catalysis 203:82-86
Okuda-Shimazaki J, Takaku S, Kanehira K, Sonezaki S, Taniguchi A (2010) Effects of titanium dioxide nanoparticle aggregate size on gene expression International journal of molecular sciences 11:2383-2392
Ong KJ et al. (2014) Widespread nanoparticle-assay interference: implications for nanotoxicity testing PLoS One 9:e90650
Ou H-H, Lo S-L (2007) Review of titania nanotubes synthesized via the hydrothermal treatment: fabrication, modification, and application Separation and Purification Technology 58:179-191
Palmas S, Da Pozzo A, Mascia M, Vacca A, Ardu A, Matarrese R, Nova I (2011) Effect of the preparation conditions on the performance of TiO2 nanotube arrays obtained by electrochemical oxidation International Journal of Hydrogen Energy 36:8894-8901 doi:https://doi.org/10.1016/j.ijhydene.2011.04.105
Panaitescu E, Richter C, Menon L (2008) A study of titania nanotube synthesis in chloride-ion-containing media Journal of The Electrochemical Society 155:E7-E13
Paramasivam I, Macak JM, Ghicov A, Schmuki P (2007) Enhanced photochromism of Ag loaded self-organized TiO2 nanotube layers Chemical Physics Letters 445:233-237 doi:https://doi.org/10.1016/j.cplett.2007.07.107
Patravale V, Dandekar P, Jain R (2012) 4 - Nanotoxicology: evaluating toxicity potential of drug-nanoparticles. In: Nanoparticulate Drug Delivery. Woodhead Publishing, pp 123-155. doi:https://doi.org/10.1533/9781908818195.123
Paulose M et al. (2006) Anodic growth of highly ordered TiO2 nanotube arrays to 134 µm in length The Journal of Physical Chemistry B 110:16179-16184

Petković J, Žegura B, Filipič M Influence of TiO2 nanoparticles on cellular antioxidant defense and its involvement in genotoxicity in HepG2 cells. In: Journal of Physics: Conference Series, 2011. vol 1. IOP Publishing, p 012037

Rahna N, Kalarivalappil V, Nageri M, Pillai SC, Hinder SJ, Kumar V, Vijayan BK (2016) Stability studies of PbS sensitised TiO2 nanotube arrays for visible light photocatalytic applications by X-ray photoelectron spectroscopy (XPS) Materials Science in Semiconductor Processing 42:303-310

Ray PC, Yu H, Fu PP (2009) Toxicity and environmental risks of nanomaterials: challenges and future needs Journal of Environmental Science and Health Part C 27:1-35

Richter C, Panaitescu E, Willey R, Menon L (2007) Titania nanotubes prepared by anodization in fluorine-free acids Journal of materials research 22:1624-1631

Ruan C, Paulose M, Varghese OK, Mor GK, Grimes CA (2005) Fabrication of highly ordered TiO2 nanotube arrays using an organic electrolyte The Journal of Physical Chemistry B 109:15754-15759

Safi M, Sarrouj H, Sandre O, Mignet N, Berret J-F (2010) Interactions between sub-10-nm iron and cerium oxide nanoparticles and 3T3 fibroblasts: the role of the coating and aggregation state Nanotechnology 21:145103

Shi H, Magaye R, Castranova V, Zhao J (2013) Titanium dioxide nanoparticles: a review of current toxicological data Particle and fibre toxicology 10:15

Sing KS (1985) Reporting physisorption data for gas/solid systems with special reference to the determination of surface area and porosity (Recommendations 1984) Pure and applied chemistry 57:603-619

Singh S et al. (2007) Endocytosis, oxidative stress and IL-8 expression in human lung epithelial cells upon treatment with fine and ultrafine TiO2: role of the specific surface area and of surface methylation of the particles Toxicology and applied pharmacology 222:141-151

Tilly TB, Kerr LL, Braydich-Stolle LK, Schlager JJ, Hussain SM (2014) Dispersions of geometric TiO2 nanomaterials and their toxicity to RPMI 2650 nasal epithelial cells Journal of nanoparticle research 16:2695

Tsai C-C, Teng H (2004) Regulation of the physical characteristics of titania nanotube aggregates synthesized from hydrothermal treatment Chemistry of Materials 16:4352-4358

Tsaryk R, Peters K, Unger R, Feldmann M, Hoffmann B, Heidenau F, Kirkpatrick C (2013) Improving cytocompatibility of Co28Cr6Mo by TiO2 coating: gene expression study in human endothelial cells Journal of The Royal Society Interface 10:20130428

Tsuchiya H et al. (2006) Hydroxyapatite growth on anodic TiO2 nanotubes Journal of Biomedical Materials Research Part A 77A:534-541 doi:10.1002/jbm.a.30677

Tsuchiya H, Macak JM, Taveira L, Balaur E, Ghicov A, Sirotna K, Schmuki P (2005) Self-organized TiO2 nanotubes prepared in ammonium fluoride containing acetic acid electrolytes Electrochemistry Communications 7:576-580 doi:https://doi.org/10.1016/j.elecom.2005.04.008

Uboldi C, Urbán P, Gilliland D, Bajak E, Valsami-Jones E, Ponti J, Rossi F (2016) Role of the crystalline form of titanium dioxide nanoparticles: Rutile, and not anatase, induces toxic effects in Balb/3T3 mouse fibroblasts Toxicology In Vitro 31:137-145

Varghese OK, Gong D, Paulose M, Grimes CA, Dickey EC (2003) Crystallization and high-temperature structural stability of titanium oxide nanotube arrays Journal of Materials Research 18:156-165

Vijayan B, Dimitrijevic NM, Rajh T, Gray K (2010) Effect of calcination temperature on the photocatalytic reduction and oxidation processes of hydrothermally synthesized titania nanotubes The Journal of Physical Chemistry C 114:12994-13002

Wang R et al. (1998) Photogeneration of Highly Amphiphilic TiO2 Surfaces Advanced Materials 10:135-138 doi:10.1002/(sici)1521-4095(199801)10:2<135::aid-adma135>3.0.co;2-m

Wang S, Lu W, Tovmachenko O, Rai US, Yu H, Ray PC (2008) Challenge in understanding size and shape dependent toxicity of gold nanomaterials in human skin keratinocytes Chemical physics letters 463:145-149

Wang X, Li Z, Shi J, Yu Y (2014) One-dimensional titanium dioxide nanomaterials: nanowires, nanorods, and nanobelts Chemical reviews 114:9346-9384

Weir A, Westerhoff P, Fabricius L, Hristovski K, Von Goetz N (2012) Titanium dioxide nanoparticles in food and personal care products Environmental science & technology 46:2242-2250

Wörle-Knirsch J, Pulskamp K, Krug H (2006) Oops they did it again! Carbon nanotubes hoax scientists in viability assays Nano letters 6:1261-1268

Wu L, Yang X, Li J, Huang Y, Li X (2017) Fabrication of titanium dioxide nanotubes with good morphology at high calcination temperature and their photocatalytic activity Materials Chemistry and Physics 202:136-142

Xia T et al. (2006) Comparison of the abilities of ambient and manufactured nanoparticles to induce cellular toxicity according to an oxidative stress paradigm Nano letters 6:1794-1807

Xia T et al. (2008) Comparison of the mechanism of toxicity of zinc oxide and cerium oxide nanoparticles based on dissolution and oxidative stress properties ACS nano 2:2121-2134

Xiong S et al. (2013) Specific surface area of titanium dioxide (TiO2) particles influences cyto-and photo-toxicity Toxicology 304:132-140

Xue C, Wu J, Lan F, Liu W, Yang X, Zeng F, Xu H (2010) Nano titanium dioxide induces the generation of ROS and potential damage in HaCaT cells under UVA irradiation Journal of nanoscience and nanotechnology 10:8500-8507

Yin ZF, Wu L, Yang HG, Su YH (2013) Recent progress in biomedical applications of titanium dioxide Physical chemistry chemical physics 15:4844-4858

Yu J, Wang B (2010) Effect of calcination temperature on morphology and photoelectrochemical properties of anodized titanium dioxide nanotube arrays Applied Catalysis B: Environmental 94:295-302

Zhang J et al. (2017) Porous TiO2 Nanotubes with Spatially Separated Platinum and CoOx Cocatalysts Produced by Atomic Layer Deposition for Photocatalytic Hydrogen Production Angewandte Chemie International Edition 56:816-820

Zhang Z, Yates Jr JT (2012) Band bending in semiconductors: chemical and physical consequences at surfaces and interfaces Chemical reviews 112:5520-5551

Zhu K, Neale NR, Miedaner A, Frank AJ (2007) Enhanced charge-collection efficiencies and light scattering in dye-sensitized solar cells using oriented TiO2 nanotubes arrays Nano letters 7:69-74

Zhu Y, Eaton JW, Li C (2012) Titanium dioxide (TiO2) nanoparticles preferentially induce cell death in transformed cells in a Bak/Bax-independent fashion PloS one 7:e50607

Cite this article as Dervin, Saoirse, Eugen Panaitescu, Latika Menon, Steven S. Hinder, Suresh C. Pillai, and Mary Garvey. "In vitro pulmonary toxicity of thermally processed titania nanotubes." *Journal of Nanoparticle Research* 22, no. 1 (2020): 1-15. https://doi.org/10.1007/s11051-019-4722-z